ARCHIVES OF ELECTRICAL ENGINEERING VOL. 71(1), pp. 211 –225 (2022)

DOI 10.24425/aee.2022.140206

Dual-mode control magnetically-coupled energy storage inductor boost inverter for renewable energy

YIWEN CHEN[1], SIXU LUO[1], ZHILIANG HUANG[2], JIAHUI JIANG[3] ✉

[1] *Fujian Key Laboratory of New Energy Generation and Power Conversion, Fuzhou University*
China

[2] *Texas Instruments Semiconductor Technologies (Shanghai) Co., Ltd.*
China

[3] *College of Electrical Engineering, Qingdao University*
China

e-mail: qdujiangjiahui@sina.com

(Received: 02.07.2021, revised: 27.09.2021)

Abstract: A novel magnetically-coupled energy storage inductor boost inverter circuit for renewable energy and the dual-mode control strategy with instantaneous value feedback of output voltage are proposed. In-depth research and analysis on the circuit, control strategy, voltage transmission characteristics, etc., providing the parameter design method of magnetically-coupled energy storage inductors and output filter. The circuit topology is cascaded by the input source V_{in}, the input filter C_{in}, a single-phase inverter bridge with a magnetically-coupled energy storage inductor, and a *CL* filter; The control strategy serves the output voltage as a reference to achieve the switch of step-down and step-up modes smoothly. The simulation results of a 1000 VA 100–200 VDC, 220 V 50 Hz AC inverter show that the proposed inverter can realize single-stage boost power conversion, which can adapt to resistive, capacitive and inductive loads, has high power density and low output waveform distortion. It has good application prospects in small and medium-capacity single-phase inverter occasions with low input voltage.

Key words: inter-harmonic, parameter identification, power system, synchrosqueezed transform, time-frequency analysis

1. Introduction

With the increasing tension around the use of major energy sources like oil, coal and natural gas, special attention is being paid to the development and utilization of new energy sources. The DC-AC inverter has a wide range of applications where DC power is converted from other new

energy sources such as DC generators, batteries, solar cells, fuel cells, and wind power [1–7]. From the perspective of circuit topology, it is usually divided into the boost inverter, buck inverter, and buck-boost inverter. The buck inverter has the characteristics of step-down, low reliability when the load is short-circuited and large output capacity [8, 9]. The boost inverter has the characteristics of step-up, high reliability when the load is short-circuited and has large output capacity [10–12]. The buck-boost inverter has the ability of buck-boost, high reliability when the load is short-circuited and has small output capacity.

In the case of low input voltage, the boost capability of inverters is demanding. The boost inverter has the following three types of schemes:

1. The traditional low-frequency link (LFL) buck circuit structure, such as a full-bridge, half-bridge and push-pull inverter, whose output terminal is connected to a step-up power frequency transformer. It has the characteristics of high conversion efficiency, large capacity, large noise, high cost and electrical isolation between input and output [13].
2. High-frequency link (HFL) circuit structure, such as a two-stage HFL inverter composed of a DC converter and SPWM inverter bridge, a quasi-single-stage HFL inverter cascaded with a DC converter and polarity reversal inverter bridge, an HFL inverter composed of two identical bidirectional DC choppers in differential form, which has the features of high conversion efficiency, small capacity and low weight, but high cost [14–16].
3. Non-isolated inverse circuit structure, such as the combined boost and buck-boost DC converter type circuit structure, consisting of two non-isolated bidirectional DC converters that output inverted low-frequency (LF) sinusoidal pulsating DC voltage in parallel with the input terminals and the output terminals in reverse series. The structure has the defect regarding the current circulating between two DC converters, unsatisfactory conversion efficiency and a large number of components [17, 19]. Single-stage Z-source and quasi-Z-source inverter circuit structure, with high output waveform quality, high reliability and impedance, but the capacity and weight are relatively large [20, 21].

In order to overcome the shortcomings of the above-mentioned boost inverter scheme, this paper proposes a dual-mode control magnetically-coupled energy storage inductor boost inverter. The inverter connects the two coils of the inductor in series on the two inverter bridge arms. During the step-up mode, a single coil can realize the magnetization and demagnetization of the core independently, which satisfies the working principle of the boost converter. In the step-down mode, two coils are required to work alternately, respectively responsible for the magnetization and demagnetization of the core, to meet the magnetic balance of the circuit. The paper presents research on the topology of the inverter, control strategy, voltage transmission characteristics, coupled energy storage inductor, filter parameter design and other key issues, finally, gives the results of circuit simulation.

2. Circuit topology and mode of magnetically-coupled energy storage inductor boost inverter

2.1. Circuit topology

The circuit topology of a magnetically-coupled energy storage inductor boost inverter is shown in Fig. 1. The circuit is composed of the cascaded input source V_{in}, the input filter C_{in}, a single-phase inverter bridge with a magnetically-coupled energy storage inductor, and a *CL*

filter. This single-phase inverter bridge consists of magnetically-coupled energy storage inductors and 4 four-quadrant power switches. Among them, the coupled inductance $L_1 = L_2 = L$, and the four-quadrant power switch is composed of two MOSFET in reverse series which has the ability to withstand bidirectional voltage stress and bidirectional current stress. The inverter achieves the inversion and the two-way power flow by adjusting the combination of the corresponding duty cycle and the switching states of the inverter.

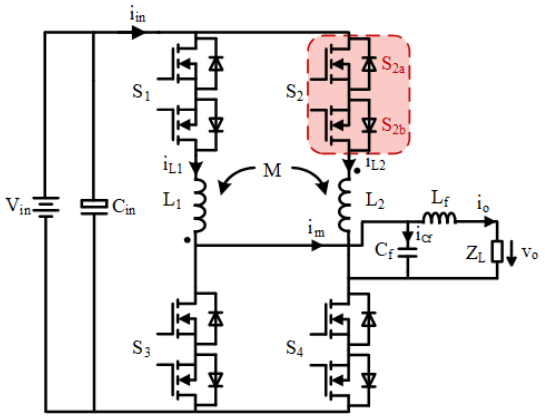

Fig. 1. Magnetically-coupled energy storage inductor boost inverter circuit topology

2.2. Circuit mode

For the coupled inductors L_1 and L_2, it may be assumed that the magnetic core is in a positive magnetization state when the inductor current i_{L1} increases, and the magnetic core is in a negative magnetization state (positive demagnetization) when i_{L2} increases. The proposed inverter has four circuit modes: L_1 magnetization mode with positive core magnetization, L_2 magnetization mode with negative core magnetization, L_1 feeding mode, and L_2 feeding mode.

The L_1 magnetization mode is shown in Fig. 2(a). At this time, the switches S_{1a}, S_{1b}, S_{3a}, and S_{3b} are turned on, and the magnetic core is in positive magnetization by V_{in} through the left bridge arm and L_1. The load is supplied by the output filter.

The L_2 magnetization mode is shown in Fig. 2(b). At this time, the switches S_{1a}, S_{1b}, S_{4a}, and S_{4b} are turned on, and the magnetic core is in negative magnetization by V_{in} through the right bridge arm and L_2. The load is supplied by the output filter.

The L_1 feeding mode is shown in Fig. 2(c). At this time, the switches S_{2a}, S_{2b}, S_{4a}, and S_{4b} are turned on. V_{in} and L_1 provide energy to the load through the inverter bridge. When $V_{\text{in}} < v_o$, the magnetic core is in positive demagnetization. When $V_{\text{in}} > v$, the magnetic core is in positive magnetization.

The L_2 feeding mode is shown in Fig. 2(d). At this time, the switches S_{2a}, S_{2b}, S_{3a}, and S_{3b} are turned on. V_{in} and L_2 provide energy to the load through the inverter bridge. When $V_{\text{in}} < -v_o$, the magnetic core is in negative demagnetization; when $V_{\text{in}} > -v_o$, the magnetic core is in the negative magnetization.

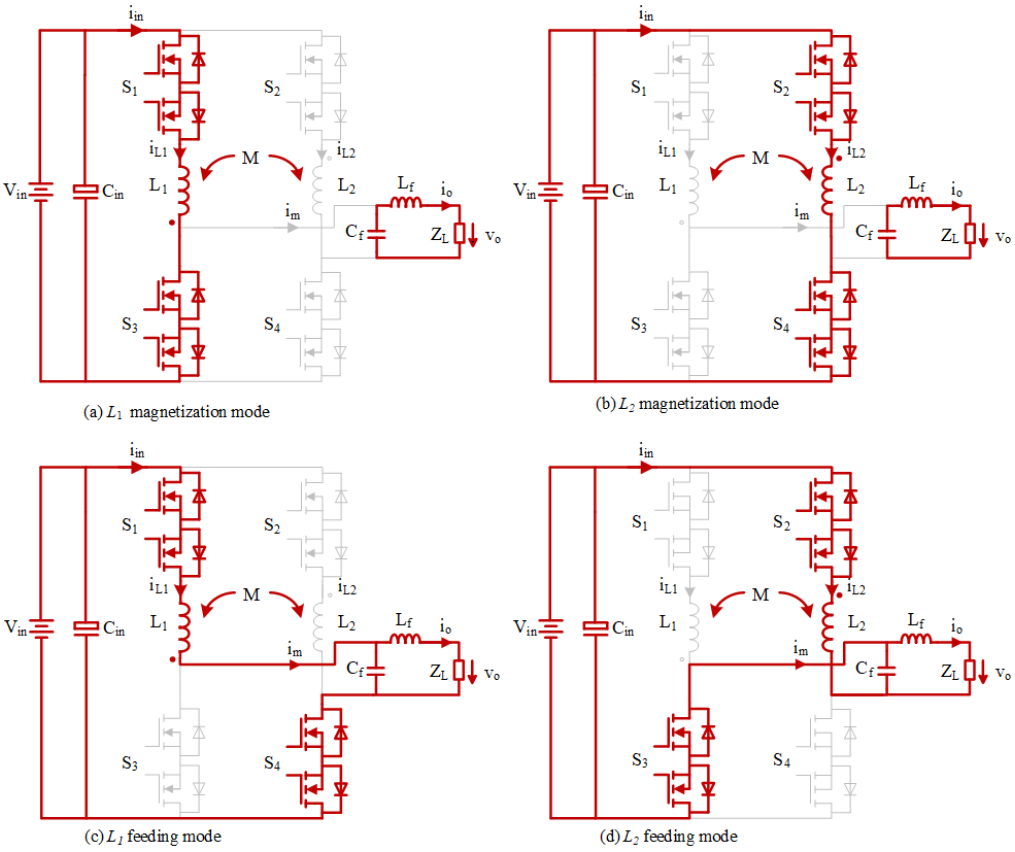

Fig. 2. Modal diagram of magnetically-coupled energy storage inductor boost inverter: L_1 magnetization mode (a); L_2 magnetization mode (b); L_1 feeding mode (c); L_2 feeding mode (d)

3. Operating mode and control strategy of magnetically-coupled energy storage inductor boost inverter

3.1. Operating mode

According to the feature of the four circuit modes, considering the magnetic balance of the core, the operating mode of the inverter in an LF output cycle can be divided into step-up mode and step-down mode.

When $V_{\text{in}} > |v_o|$, the inverter works in step-down mode. Each high-frequency (HF) switching period T_s of this mode includes $L_2(L_1)$ magnetization mode in the period of D_1T_s and $L_1(L_2)$ feeding mode in the period of $(1 - D_1 - D_2)T_s$ ($D_2 = 0$ in step-down mode). If $v_o > 0$, L_2 and L_1 work in magnetization mode and feeding mode, respectively; if $v_o < 0$, L_1 and L_2 work in magnetization mode and feeding mode, respectively. L_1 and L_2 work alternately in each T_s of this mode.

When $V_{\text{in}} < |v_o|$, the inverter works in step-up mode. Each HF switching period T_s of this mode includes $L_1(L_2)$ magnetization mode in the period of D_2T_s and $L_1(L_2)$ feeding mode in the period of $(1 - D_1 - D_2)T_s$ ($D_1 = 0$ in step-up mode). If $v_o > 0$, only L_1 works; if $v_o < 0$, only L_2 works.

It can be seen that the positive half-cycle of v_o has L_1 magnetization mode, L_2 magnetization mode and L_1 feeding mode, where the L_1 feeding mode appears in each T_s; Similarly, the negative half-cycle of v_o has L_1 magnetization mode, the L_2 magnetization mode and the L_2 feed mode, where the L_2 feed mode appears in each T_s.

3.2. Dual mode control strategy

The magnetically-coupled energy storage inductor boost inverter adopts the step-up and step-down dual-mode control strategy with instantaneous value feedback of output voltage, and the strategy is shown in Fig. 3. In step-down mode, S_1 and S_2 work in complementary conduction at HF while S_3 and S_4 work in complementary conduction at LF in positive and negative half cycle of v_o. D_2 is 0 and D_1 decreases as v_o rises. The inductor current i_{L1} and i_{L2} are complementary

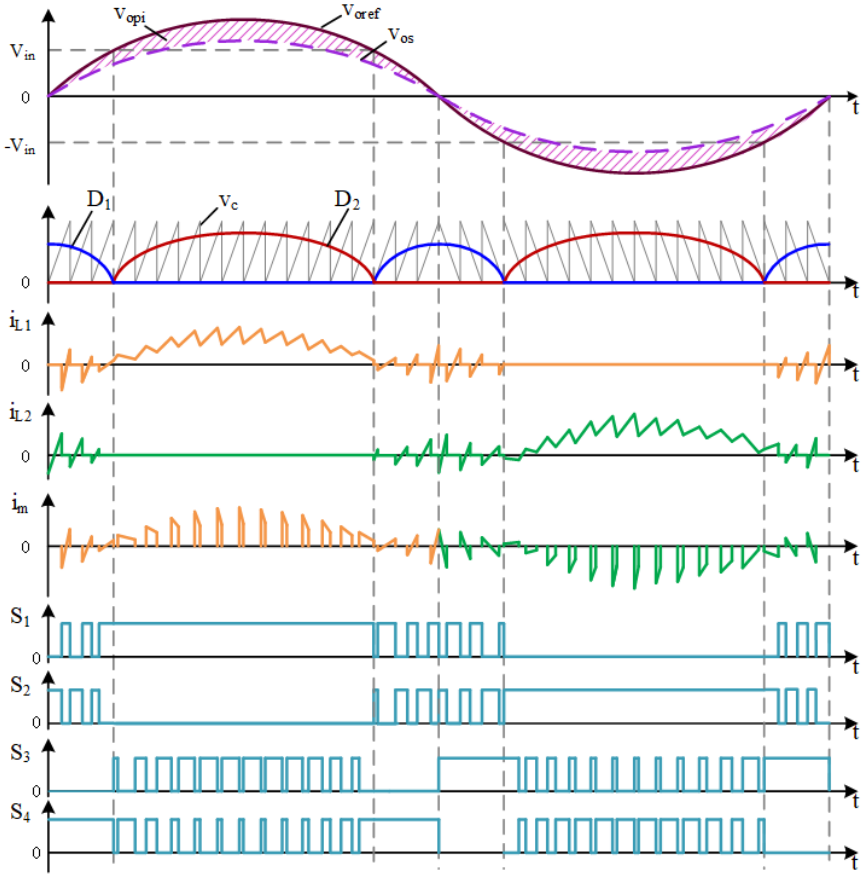

(a)

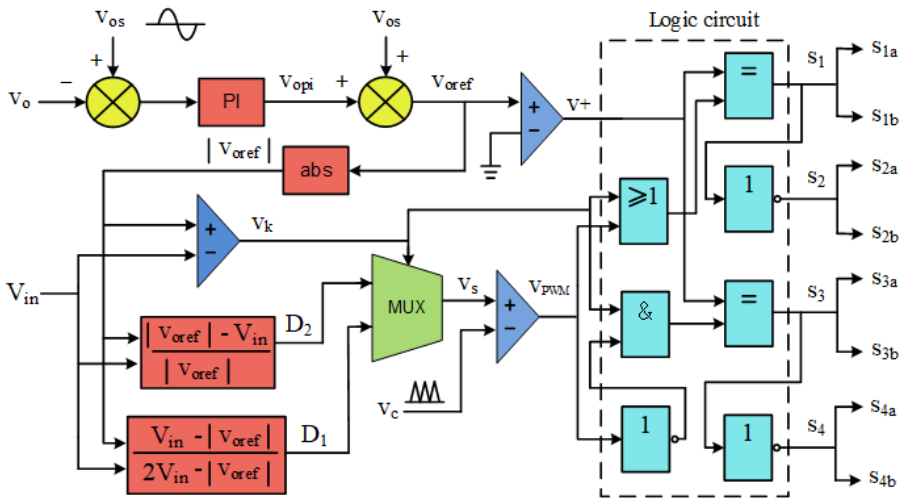

(b)

Fig. 3. Dual-mode control strategy based on instantaneous value feedback of output voltage: control principle waveform (a); control block diagram (b)

intermittently. The modulation currenti_m is equal to the inductor current; In step-up mode, S_1 and S_2 work in complementary conduction at LF while S_3 and S_4 work in complementary conduction at HF in positive and negative half-cycle of the output voltage. $D_1 = 0$ and D_2 increases as v_o rises. The coupled inductors L_1, L_2 conduct at LF in positive and negative half-cycles of the output voltage, i_m is equal to the feeding inductor current. In addition, the polarity of v_{oref} is served as the basis of output positive and negative half-cycle voltages. In Fig. 3, v_{os} is the output voltage reference value, v_{oref} is the calculation reference value, v_+ is the output waveform polarity judgment signal, v_k is the step-up or step-down mode signal, and v_{PWM} is the feed signal. Table 1 shows the relationship between the control signal and the power switch drive signal in the control block diagram.

Table 1. The relationship between control signal and power switch drive signal of inverter

v_+	v_k	v_{PWM}	S_1	S_2	S_3	S_4
1	1	1	1	0	0	1
1	1	0	1	0	1	0
1	0	1	1	0	0	1
1	0	0	0	1	0	1
0	1	1	0	1	1	0
0	1	0	0	1	0	1
0	0	1	0	1	1	0
0	0	0	1	0	1	0

4. Voltage transmission characteristics of magnetically-coupled energy storage inductor boost inverter

The circuit modes of the magnetically-coupled energy storage inductor boost inverter are symmetrical in the positive and negative half-cycles of the output voltage, and there are three circuit modes in each half cycle. The equivalent circuits of these three circuit modes in the positive half-cycle are shown in Fig. 4.

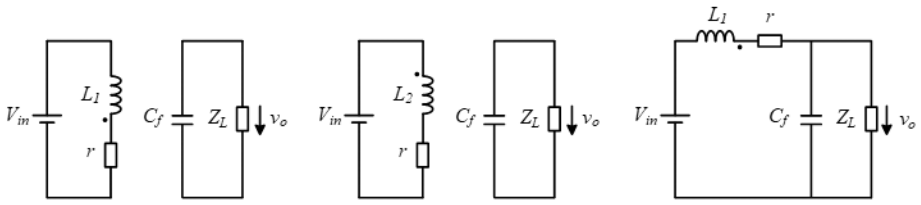

(a) (b) (c)

Fig. 4. Circuit modal equivalent circuit diagram: L_1 magnetization equivalent mode (a); L_2 magnetization equivalent mode (b); L_1 feeding equivalent mode (c)

The state equation of L_1 magnetization mode is:

$$\begin{aligned} N\frac{\mathrm{d}\varphi}{\mathrm{d}t} + \frac{\varphi}{L}r &= V_{\text{in}} \\ C_f\frac{\mathrm{d}v_o}{\mathrm{d}t} + \frac{v_o}{R_L} &= 0 \end{aligned}. \tag{1}$$

The state equation of L_2 magnetization mode is:

$$\begin{aligned} N\frac{\mathrm{d}\varphi}{\mathrm{d}t} + \frac{\varphi}{L}r &= -V_{\text{in}} \\ C_f\frac{\mathrm{d}v_o}{\mathrm{d}t} + \frac{v_o}{R_L} &= 0 \end{aligned}. \tag{2}$$

The state equation of L_1 feeding mode is:

$$\begin{aligned} N\frac{\mathrm{d}\varphi}{\mathrm{d}t} + \frac{\varphi}{L}r &= V_{\text{in}} - v_o \\ C_f\frac{\mathrm{d}v_o}{\mathrm{d}t} + \frac{v_o}{R_L} &= \frac{\varphi}{L} \end{aligned}. \tag{3}$$

In the formula: φ is the magnetic flux of magnetic core; N is the number of coil turns of L_1 and L_2; r is the equivalent resistance including the inductor winding, the power switch and the diode on-state resistance.

According to the conservation of magnetic flux and the average value of v_o during a high HF cycle, the voltage transfer ratio M can be obtained as:

$$M = \frac{(1-2D_1)(1-D_1-D_2)R_L}{r+(1-D_1-D_2)^2R_L}. \tag{4}$$

It can be seen from Eq. (4) that the voltage range theoretically depends on the maximum voltage transfer ratio $M_{\max}$ of the inverter in the step-mode ($D_1 = 0$). If the set resistance is $r = 0.25\ \Omega$ and load $R_L = 48.4\ \Omega$, then the maximum voltage transfer ratio is 6.95 when $D_2 = 0.928$. Considering the utilization rate of the step-up mode, the maximum range of D_2 is limited to 0.40 to 0.70, and the range of $M_{\max}$ is 1.64 to 3.15. When $V_m = 311$ V, the output voltage range of the proposed inverter is about 100 V to 200 V.

Suppose that

$$v_{o\text{ref}} = V_m \sin(\omega_0 t + \theta_0), \qquad \theta_1 = \arcsin\frac{V_{\text{in}}}{V_m}, \qquad k = 0, 1, 2, 3, \ldots .$$

When neglecting the resistance r, the inductor magnetizing duty ratios $D_1(t)$ and $D_2(t)$ are:

$$D_1(t) = \begin{cases} \dfrac{V_{\text{in}} - |V_m \sin(\omega_0 t + \theta_0)|}{2V_{\text{in}} - |V_m \sin(\omega_0 t + \theta_0)|} & t \in \left(k\pi, k\pi + \dfrac{\theta_1 - \theta_0}{\omega_0}\right) \cup \left(k\pi + \pi - \dfrac{\theta_1 - \theta_0}{\omega_0},\ k\pi + \pi\right) \\ 0 & t \in \left(k\pi + \dfrac{\theta_1 - \theta}{\omega_0},\ k\pi + \pi - \dfrac{\theta_1 - \theta_0}{\omega_0}\right) \end{cases}, \quad (5)$$

$$D_2(t) = \begin{cases} 0 & t \in \left(k\pi,\ k\pi + \dfrac{\theta_1 - \theta_0}{\omega_0}\right) \cup \left(k\pi + \pi - \dfrac{\theta_1 - \theta_0}{\omega_0},\ k\pi + \pi\right) \\ \dfrac{|V_m \sin(\omega_0 t + \theta_0)| - V_{\text{in}}}{|V_m \sin(\omega_0 t + \theta_0)|} & t \in \left(k\pi + \dfrac{\theta_1 - \theta_0}{\omega_0},\ k\pi + \pi - \dfrac{\theta_1 - \theta_0}{\omega_0}\right) \end{cases}. \quad (6)$$

Eqs. (5) and (6) indicate that $D_1 = 0$ in the step-up mode and $D_2 = 0$ in the step-down mode.

5. Design of coupled energy storage inductor

For the step-down mode, taking the positive half-cycle of the output voltage as an instance, the waveforms of the coupled inductor currents i_{L1}, i_{L2} and the core magnetic flux φ in an HF switching period are shown in Fig. 5. In the duration of $(0, D_1 T_s)$, the circuit works in the L_2 magnetization mode. The core is magnetized in the negative direction and the inductor current

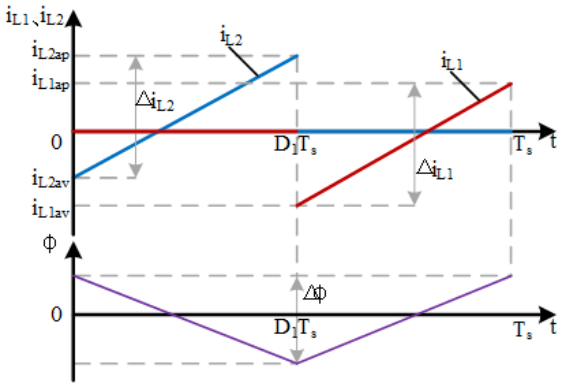

Fig. 5. The change of high-frequency period inductor current and magnetic core flux

$i_{L1} = 0$, i_{L2} rises; In the duration of (D_1T_s, T_s), the circuit works in the L_1 feeding mode, the core is magnetized in the positive direction, the inductor current i_{L1} rises, $i_{L2} = 0$.

In an HF cycle, the variation of the currents Δi_{L1} and Δi_{L2} are respectively:

$$\Delta i_{L1} = \Delta i_{L2} = \frac{D_1 \cdot T_s \cdot V_{\text{in}}}{L} . \tag{7}$$

According to the magnetic potential balance, the peak and valley values of i_{L1} and i_{L2} have the following relationship:

$$i_{L2av} = -i_{L1ap} , \tag{8}$$

$$i_{L2ap} = -i_{L1av} . \tag{9}$$

The average value of the input current I_{in} in an HF cycle:

$$I_{\text{in}} = (1 - 2D_1) \cdot \left[i_{L1av} + \frac{D_1 \cdot T_s \cdot V_{\text{in}}}{2L} \right] . \tag{10}$$

It can be obtained from the conservation of power:

$$I_{\text{in}} = \frac{v_o i_o}{V_{\text{in}}} . \tag{11}$$

Through Formulas (5), (10) and (11), the peak and valley values i_{L1ap} and i_{L1av} of the inductor current in an HF cycle in the step-down mode can be obtained:

$$i_{L1ap} = p_o \cdot \frac{2V_{\text{in}} - v_o}{v_o \cdot V_{\text{in}}} + \frac{T_s \cdot V_{\text{in}} \cdot (V_{\text{in}} - v_o)}{2L \cdot (2V_{\text{in}} - v_o)}, \tag{12}$$

$$i_{L1av} = p_o \cdot \frac{2V_{\text{in}} - v_o}{v_o \cdot V_{\text{in}}} - \frac{T_s \cdot V_{\text{in}} \cdot (V_{\text{in}} - v_o)}{2L \cdot (2V_{\text{in}} - v_o)}. \tag{13}$$

The inverter in the step-up mode is equivalent to the operating state of the boost converter. Taking the output positive half-cycle as an example, the peak value, valley value i_{L1bp} and i_{L1bv} of the inductor current in an HF switching cycle are respectively:

$$i_{L1bp} = \frac{p_o}{V_{\text{in}}} + \frac{T_s \cdot V_{\text{in}} \cdot (v_o - V_{\text{in}})}{2L \cdot v_o} , \tag{14}$$

$$i_{L1bv} = \frac{p_o}{V_{\text{in}}} - \frac{T_s \cdot V_{\text{in}} \cdot (v_o - V_{\text{in}})}{2L \cdot v_o} . \tag{15}$$

It can be seen from Eqs. (12), (13) that in the step-down mode, the inductor current is the largest when the circuit is fully loaded, $\cos\varphi = 0.75$ and $v_o = 0$. From Eqs. (14), (15), it can be seen that the inductor current is the largest in the step-up mode when the circuit is fully loaded, $\cos\varphi = 1$ and $v_o = V_m$. Considering that the steady-state component and fluctuations of the inductor current in the step-up mode are greater than those in the step-down mode, thus the maximum inductor current in an LF cycle occurs at the moment when the output power is the maximum in the resistive full-load step-up mode. Suppose the maximum value of the inductor current is $i_{L\,\max}$, then the inductance satisfies:

$$L \geq \frac{V_{\text{in}} \cdot T_s \cdot (V_m - V_{\text{in}})}{2V_m \cdot \left(i_{L\,\max} - \dfrac{P_{o\,\max}}{V_{\text{in}}} \right)} . \tag{16}$$

6. Output *CL* filter design

The output side of the proposed inverter adopts a *CL* filter. It can be seen from Fig. 1 that the relationship between i_m and v_o is

$$i_m = \frac{v_o}{Z_L} + \frac{C_f L_f}{Z_L}\frac{\mathrm{d}^2 v_o}{\mathrm{d}t^2} + C_f \frac{\mathrm{d}v_o}{\mathrm{d}t}. \tag{17}$$

Therefore, the transfer function $G(s)$ from v_o to i_m is

$$G(s) = \frac{V_o(s)}{I_m(s)} = \frac{Z_L \cdot \omega_n^2}{s^2 + 2\xi\omega_n s + \omega_n^2}, \tag{18}$$

where the natural oscillation frequency and damping ratio of the filter are

$$\begin{cases} \omega_n = \dfrac{1}{\sqrt{L_f C_f}} \\ \xi = \dfrac{Z_L\sqrt{L_f C_f}}{2} \end{cases}.$$

ω_n of the filter, the switching frequency f_s and the output voltage frequency f_0 need to satisfy:

$$10 f_0 \le \frac{\omega_n}{2\pi} \le 0.1 f_s\,. \tag{19}$$

7. Simulation analysis

Simulation has been performed for the proposed circuit using circuit simulation software (PSIM). The simulation parameters are as follows: rated capacity $S = 1000$ VA, input voltage $V_{\text{in}} = 100$–200 V, output voltage $V_o = 220$ V/50 Hz AC, power factor $\cos\varphi$ is capacitive 0.75–1 – inductive 0.75, switching frequency $f_s = 50$ kHz, an input filter capacitor $C_{in} = 220$ µF, output filter inductance $L_f = 1$ mH, an output filter capacitor $C_f = 10$ µF, inductance $L_1 = L_2 = 0.2$ mH. According to the capacity of the circuit, the voltage and current stress of the device and the corresponding device parameters, in the simulation, the on-state resistance of each switch is set to 60 mΩ, the equivalent junction capacitance of the switch is 280 pF, and the equivalent resistance of each winding coil of the coupled inductor is 10 mΩ.

Figure 6 is the simulation waveform diagram of the inverter. The simulation results indicate that:

1. The ideal drain-source voltage envelopes of S_{1a}, S_{1b}, S_{2a}, and S_{2b} in step-up and step-down modes are $2V_{\text{in}} + v_o$ and $2V_{\text{in}} - v_o$, respectively. In the simulation, the drain-source voltage is relatively high due to leakage inductance. The drain-source voltage envelope of S_{3a}, S_{3b}, S_{4a}, andS_{4b} is v_o.
2. The waveforms of i_{L1} and i_{L2} are consistent with the theoretical results, whose maximum value falls within the designed 25 A.
3. In Figs. 6(d)–(f), the inverter performs well with resistive, capacitive and inductive loads. The output voltage THD is 1.45%, 1.56% and 1.84%, and the output current THD is 1.45%, 2.02% and 0.61%.

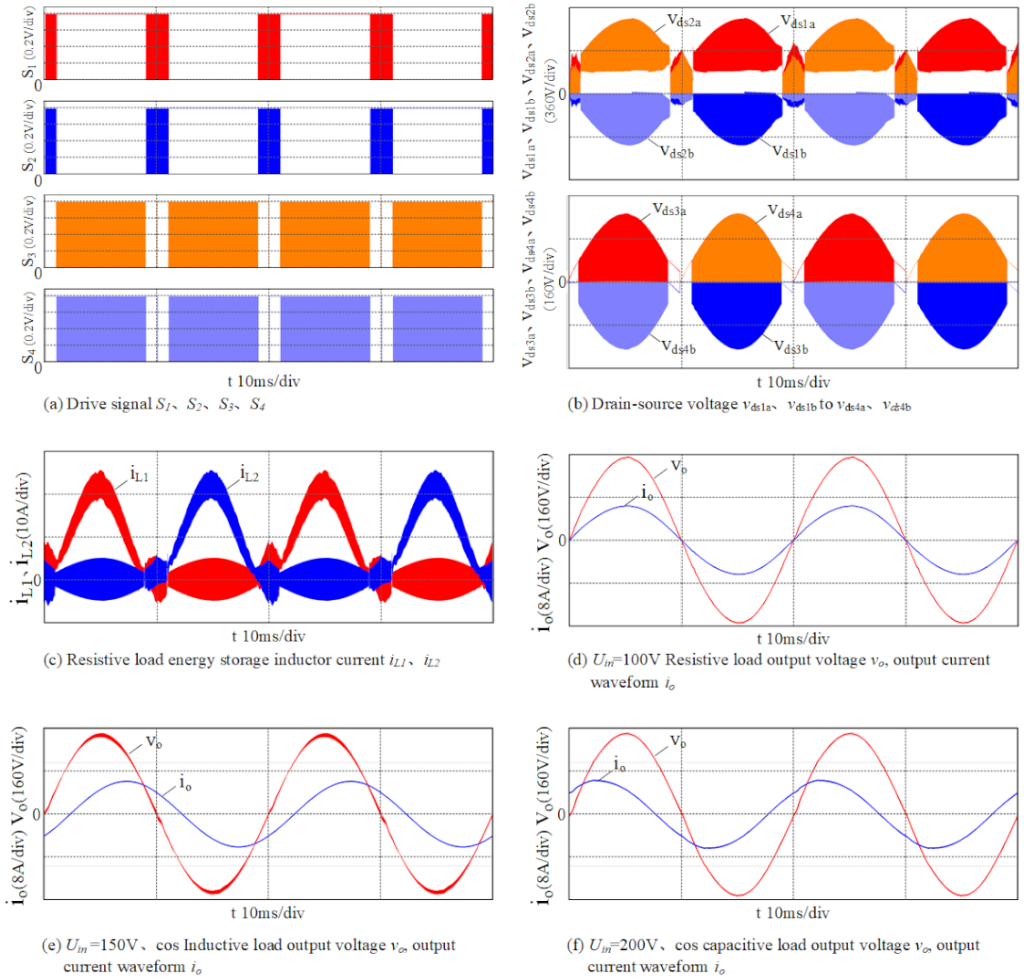

Fig. 6. Full-load steady-state simulation waveform of the inverter: drive signals S_1, S_2, S_3, S_4 (a); drain-source voltage v_{ds1a}, v_{ds1b} to v_{ds4a}, v_{ds4b} (b); resistive load energy storage inductor current i_{L1}, i_{L2} (c); V_{in} = 100 V resistive load output voltage v_o, output current i_o(d); V_{in} = 150 V, cos φ = 0.75 inductive load output voltage v_o, output current i_o (e); V_{in} = 200 V, cos φ = 0.75 capacitive load output voltage v_o, output current i_o (f)

The dynamic simulation waveform of the proposed inverter is shown in Fig. 7. When the load changes from resistive half load to resistive full load, the waveform of v_o stabilizes quickly, and the dynamic response time is about 3 ms. When the input voltage V_{in} changes from 100 V to 120 V, v_o and i_o also behave well, its dynamic response time is about 2.5 ms.

Table 2 provides a comparison between the proposed inverter and the other three inverters in terms of circuit parameters and performance. It can be seen from the data in Table 2 that the output voltage THD of the proposed inverter under resistive load is 1.45%, and the efficiency is

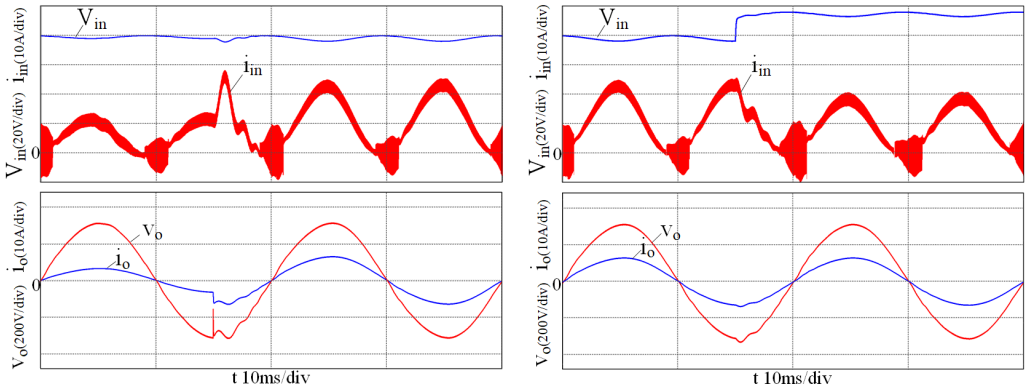

Fig. 7. Dynamic simulation waveform of the inverter: resistive half load to resistive full load (a); resistive full load V_{in} switches from 100 V to 120 V (b)

96.76%. Compared with other circuits, the proposed inverter requires fewer passive components and has higher efficiency, as well as can achieve a good output waveform through a simple control loop, but the switching voltage stress is relatively high.

Table 2. Comparison between the proposed inverter and the inverter in reference [22–24]

	Ref [22]	**Ref [23]**	**Ref [24]**	**Proposed Inverter**
Energy storage inductor	1 mH × 2	0.55 mH × 2	1 mH × 3	0.2 mH × 2
Energy storage capacitor	1 μF × 2	5 μF × 2	1 μF × 4	–
Filter inductance	1 mH	–	1.2 mH	1 mH
Filter capacitor	1 μF	–	1 μF	10 μF
Num. of switches	6	4	4	8
Num. of diodes	2	–	2	–
Maximum voltage stress	V_m	$\frac{2V_mV_{\text{in}}}{V_m+2V_{\text{in}}-\sqrt{V_m^2+4V_{\text{in}}^2}}$	$\frac{3V_m-V_{\text{in}}}{2}$	$2V_{\text{in}}+V_m$
Boost ratio	$\frac{1}{1-D}$	$\frac{1-2D}{D(1-D)}$	$\frac{1}{1-3D}$	$\frac{1}{1-D}$
THD	1.84%	1.81%	1.7%	1.45%
Efficiency	96.78%	92.5%	91.6%	96.76%

8. Conclusions

1. A novel magnetically-coupled energy storage inductor boost inverter circuit topology is proposed. The circuit is composed of the cascaded input source V_{in}, the input filter C_{in}, a single-phase inverter bridge with a magnetic coupled energy storage inductor, and a *CL* filter. This single-phase inverter bridge consists of magnetically-coupled energy storage inductors and 4 four-quadrant power switches. It has two operating modes and four circuit modes. The coupled inductor can realize the magnetic potential balance of each switching cycle in the inverter's step-up conversion and step-down conversion.
2. The dual-mode control strategy with the feedback of the instantaneous value of the output voltage can smoothly switch between the two operation modes according to the output voltage error, and the instantaneous forward and reverse power flow of resistive, capacitive and inductive loads can be achieved.
3. In-depth analysis of the voltage transmission characteristics of the inverter, calculation of the time domain value of the duty cycle, and the parameter design method of the magnetically-coupled energy storage inductor and the output filter is provided.
4. Simulation results of PSIM show that the proposed inverter can realize single-stage boost power conversion, can adapt to resistive, capacitive and inductive loads, has the characteristics of high power density, low output waveform distortion, etc., and is suitable for the wider input voltage range of small and medium power boost inverter occasions.

Acknowledgements

This work was supported by Shandong Provincial Natural Science Foundation [grant number ZR2019 QEE044].

References

[1] Hussain H.M., Narayanan A., Nardelli P.H.J., Yang Y., *What Is Energy Internet? Concepts, Technologies, and Future Directions*, IEEE Access., vol. 8, pp. 183127–183145 (2020), DOI: 10.1109/access.2020.3029251.

[2] Tao Z., Jiahui J., Daolian C., *An efficient and low-cost DMPPT approach for photovoltaic submodule based on multi-port DC converter*, Renewable Energy, vol. 178, pp. 1144–1155 (2021), DOI: 10.1016/j.renene.2021.06.134.

[3] Jiang J., Zhang T., Chen D., *Analysis, Design, and Implementation of a Differential Power Processing DMPPT With Multiple Buck–Boost Choppers for Photovoltaic Module*, IEEE Transactions on Power Electronics, vol. 36, no. 9, pp. 10214–10223 (2021), DOI: 10.1109/tpel.2021.3063230.

[4] Xianglin L., Zhiwei X., Xueyu Y., Lixia Z., Wenzhong M., Wei H., *Low-complexity multivector-based model predictive torque control for PMSM with voltage preselection*, IEEE Transactions on Power Electronics, vol. 36, no. 10, pp. 11726–11738 (2021), DOI: 10.1109/tepl.2021.3073137.

[5] Xianglin L., Zhiwei X., Lixia Z., Wei H., *A low-complexity three-vector-based model predictive torque control for SPMSM*, IEEE Transactions on Power Electronics, vol. 36, no. 11, pp. 13002–13012 (2021), DOI: 10.1109/TPEL.2016.2532387.

[6] Rahbar K., Chai C.C., Zhang R., *Energy cooperation optimization in microgrids with renewable energy integration*, IEEE Transactions on Smart Grid, vol. 9, no. 2, pp. 1482–1493 (2018), DOI: 10.1109/tsg.2016.2600863.

[7] Quint R. *et al., Transformation of the grid: the impact of distributed energy resources on bulk power systems*, IEEE Power and Energy Magazine, vol. 17, no. 6, pp. 35–45 (2019), DOI: 10.1109/mpe.2019.2933071.

[8] Salem Q., Liu L., Xie J., *Dual operation mode of a transformerless h-bridge inverter in low-voltage microgrid*, IEEE Transactions on Industry Applications, vol. 55, no. 5, pp. 5289–5299 (2019), DOI: 10.1109/tia.2019.2917807.

[9] Hanchao Z., Daolian C., *A single-stage isolated charging/discharging DC-AC converter with second harmonic current suppression in distributed generation systems*, IECON 2017 – 43rd Annual Conference of the IEEE Industrial Electronics Society, Beijing, China, pp. 4427–4432 (2017).

[10] Liu S., He Y., Wang G., Wang M., *Power Decoupling Control for Boost-Type Single-Phase Inverter with Active Power Buffer*, 2019 IEEE Energy Conversion Congress and Exposition, Maryland, USA, pp. 2280–2285 (2019).

[11] Stawiarski Ł., Piróg S., *Active power decoupling topology for AC-DC and DC-AC single-phase systems with decoupling capacitor minimization*, Archives of Electrical Engineering, vol. 67, no. 1, pp. 193–205 (2018), DOI: 10.24425/aee.2018.119001.

[12] Xu S., Chang L., Shao R., *Single-phase voltage source inverter with voltage Boosting and power decoupling capabilities*, IEEE Journal of Emerging and Selected Topics in Power Electronics, vol. 8, no. 3, pp. 2977–2988 (2020), DOI: 10.1109/jestpe.2019.2936136.

[13] Chen Z., Wu Q., Yuan Y., *A novel zero-voltage-switching push–pull high-frequency-link single-phase inverter*, IEEE Journal of Emerging and Selected Topics in Power Electronics, vol. 4, no. 2, pp. 421–434 (2016), DOI: 10.1109/jestpe.2015.2505171.

[14] Watanabe H., Itoh J., *Novel DC to single-phase AC isolated current source inverter with power decoupling capability for micro-inverter system*, 2015 IEEE Energy Conversion Congress and Exposition, Montreal, Canada, pp. 158–165 (2015).

[15] Chakraborty S., Chattopadhyay S., *An isolated Buck-Boost type high-frequency link photovoltaic microinverter*, 2016 IEEE Applied Power Electronics Conference and Exposition, California, USA, pp. 3389–3396 (2016).

[16] Jiang J., Li Z., Chen D., *A quasi single stage isolated Buck-Boost mode multi-input inverter*, 2019 10th International Conference on Power Electronics and ECCE Asia, Busan, Korea, pp. 1–6 (2019).

[17] Baoge Z., Deyu H., Tianpeng W., Zhen Z., Donghao W., *A novel two-phase interleaved parallel bi-bidirectional DC/DC converter*, Archives of Electrical Engineering, vol. 70, no. 1, pp. 219–234 (2021), DOI: 10.24425/aee.2021.136063.

[18] Hong F., Liu J., Ji B., Zhou Y., Wang J., Wang C., *Single inductor dual Buck full-bridge inverter*, IEEE Transactions on Industrial Electronics, vol. 62, no. 8, pp. 4869–4877 (2015), DOI: 10.1109/tie.2015.2399280.

[19] Zhang L., Zhang T., Hao Y., Wang B., *Two-stage dual-Buck grid-tied inverters with efficiency enhancement*, 2019 IEEE Applied Power Electronics Conference and Exposition, California, USA, pp. 3251–3256 (2019).

[20] Jagan V., Kotturu J., Das S., *Enhanced-Boost quasi-z-source inverters with two-switched impedance networks*, IEEE Transactions on Industrial Electronics, vol. 64, no. 9, pp. 6885–6897 (2017), DOI: 10.1109/tie.2017.2688964.

[21] Zhu X., Zhang B., Qiu D., *A high Boost active switched quasi-z-source inverter with low input current ripple*, IEEE Transactions on Industrial Informatics, vol. 15, no. 9, pp. 5341–5354 (2019), DOI: 10.1109/tii.2019.2899937.

[22] Leonardo P. Sampaio, Moacyr A.G. de Brito, Luigi G. Junior, *Single-phase current-source-Boost inverter for renewable energy sources*, 2011 IEEE International Symposium on Industrial Electronics, Gdansk, Poland, pp. 1118–1123 (2011), DOI: 10.1109/ISIE.2011.5984201.

[23] Nattymol Y.J., Shanavas T.N., *Power quality analysis of single-phase transformer-less Buck-Boost inverter for compressor load*, 2019 IEEE International Conference on Intelligent Techniques in Control, Optimization and Signal Processing (INCOS), Tamilnadu, India (2019), DOI: 10.1109/INCOS45849.2019.8951345.

[24] Sreekanth T., Lakshmi Narasamma N., Mahesh K. Mishra, Sijo Augustine, *A single stage coupled inductor based high gain DC-AC Buck-Boost inverter for photovoltaic (PV) applications*, 2015 IEEE 42nd Photovoltaic Specialist Conference (PVSC), New Orleans, LA, USA (2015), DOI: 10.1109/pvsc.2015.7356269.